JOURNAL OF MATERIALS SCIENCE **33** (1998) 5365–5374

Fabrication of *in situ* TiC reinforced aluminum matrix composites Part I *Microstructural characterization*

X. C. TONG
Department of Materials Science and Engineering, The University of Michigan, Ann Arbor, Michigan 48109-2136, USA

In the present work traditional ingot metallurgy plus rapid solidification techniques were used to *in situ* produce Al-TiC composites with refined microstructures and enhanced dispersion hardening of the reinforcing phases. Microstructural characterization of the experimental materials were comprehensively done by optical, electron microscopy and X-ray diffraction. The results show that the *in situ* synthesized TiC particles possess a metastable fcc crystal structure with an atomic composition of TiC_{08} and a lattice parameter of 0.431 nm. The typical ingot metallurgy microstructures exhibit aggregates of TiC particle phase segregated generally at the α-Al subgrain or grain boundaries and consisted of fine particles of 0.2–1.0 μm. After re-melting of the ingots and hence rapid solidification, the microstructures formed under certain thermal history conditions contained uniform fine-scale dispersion of TiC phase particles with a size range of 40–80 nm in an Al supersaturated matrix of 0.30–0.85 μm grain size. In the most case these dispersed TiC particles have a semi-coherent relationship with the α-Al matrix.

1. Introduction

Aluminum-based metal matrix composites (MMCs) have a high potential for advanced structural applications when high specific strength and modulus as well as good elevated temperature resistance are important [1–5]. In particular, the particulate-reinforced MMCs are of more interest due to their ease of fabrication, lower costs, and more isotropic properties. It is widely recognized that the properties of MMCs are controlled by the size and volume fraction of the reinforcement phase as well as the nature of the matrix-reinforcement interface: an optimum set of mechanical properties tends to be obtained when fine and thermally stable ceramic particulates are dispersed in a metal matrix. Traditionally, MMCs have been produced by such processing techniques as powder metallurgy, preform infiltration, spray deposition, mechanical alloying and various casting technologies, e.g. squeeze casting, rheocasting and compocasting [3, 6–9]. Such technology is based on the addition of the particulate reinforcement to the matrix materials which may be in molten or powder form. In this case the scale of the reinforcing phase is limited by the starting powder size, which is typically of the order of microns to tens of microns and rarely below 1 μm. In recent years novel processing techniques based on the *in situ* production of MMCs have emerged. *In situ* techniques involve a chemical reaction resulting in the formation of a very fine and thermodynamically stable reinforcing ceramic phase within a metal matrix. As a result, this provides thermodynamic compatibility at the matrix-reinforcement interface. The reinforcement surfaces are also likely to be free of contamination and therefore a stronger matrix-dispersoid bond can be achieved. Some of these technologies include DIMOX^{TM}, XD^{TM}, reactive gas infiltration, high temperature self-propagating synthesis (SHS) and liquid-solid or liquid-liquid reactions [10–15]. Both Al-TiC and Al-TiB_2 composites and composite powders with up to 40 vol % of fine (1 μm or less) reinforcement were reported to have been successfully produced by the XD^{TM} and SHS processes [10, 13]. Infiltration of a carbonaceous gas in a molten Al-Ti alloy was found suitable to form Al-TiC composites with a fine reinforcement size (0.1–3 μm) at low to moderate volume fractions (less than 15%) [16, 17].

Among the several techniques available to synthesize MMCs, the solidification processes where the reinforcing particles are formed *in situ* in the molten aluminum prior to its solidification are particularly attractive due to their simplicity, economy and flexibility. The judicious selection of solidification processing techniques, matrix alloy compositions, and dispersoids can produce new structures and impart a unique set of useful engineering properties to the composites that are difficult to obtain in conventional monolithic materials. Specifically, the solidification conditions that are present during processing play an important role in dictating the microstructure and the mechanical and physical characteristics of MMCs. For example, the dendrite arm spacing [18, 19], solute segregation [20, 21],

and distribution of reinforcing phases [22, 23] present in MMCs have all been shown to critically depend on the solidification conditions present during processing. However, microstructure refinement arising from rapid solidification processing (RSP) offers a potential avenue to alleviate the solute segregation and enhance the dispersion hardening by substantially reducing the size scale of the reinforcing phases and modifying their distribution in the aluminum matrix [24]. Therefore, the concept of combining the advantages of both MMCs and RSP seems significant for the development of novel materials with improved physical and mechanical properties.

In the present work, traditional ingot metallurgy plus rapid solidification techniques were used to *in situ* produce Al-TiC composites (including *in situ* TiC reinforced Al-Si and Al-Fe based composites) with refined microstructures and enhancing dispersion hardening of the reinforcing phases. The incorporation of these carbides formed *in situ* into a high strength or an elevated-temperature alloy system offers the advantage of increasing the modulus and strength of the base alloy over and above that possible through conventional techniques, while still maintaining a relatively low volume fraction to preserve the fracture toughness and elongation. This paper (Part I) gives a particular attention to the characterization of the microstructure with varying C : Ti ratios in the Al-Ti-C alloys. The Part II and Part III will give *in situ* synthesis mechanism of TiC and its evolution during rapid solidification, and mechanical properties of the Al-TiC composites, respectively.

2. Experimental

The synthesis of the composites was carried out firstly by ingot metallurgy and then rapid solidification. Master material ingots were prepared from a mixture of Al(99.9%), Ti(99.7%), and graphite powder of 40–50 μm average particle size in a graphite-lined induction furnace, with a blanket of argon gas over the melt. Initially the mixture was melted and upon reaching the processing temperature of 1373–1473 K in one hour, the temperature was increased to 1573–1623 K holding 10 minutes and subsequently direct chill cast into ingot bars with a diameter of 12 mm. Typical compositions of the ingots are given in Table I.

Chemical analysis (except for carbon) of the master ingots was done by a wet method. Carbon was determined by an automatic combustion apparatus, wherein the sample is combusted in a stream of oxygen and the carbon of the specimen is converted into CO_2, which is then fed into a measuring chamber, where the concentration peak is detected with a non-dispersive spectrometer. The linear signal is integrated and displaced

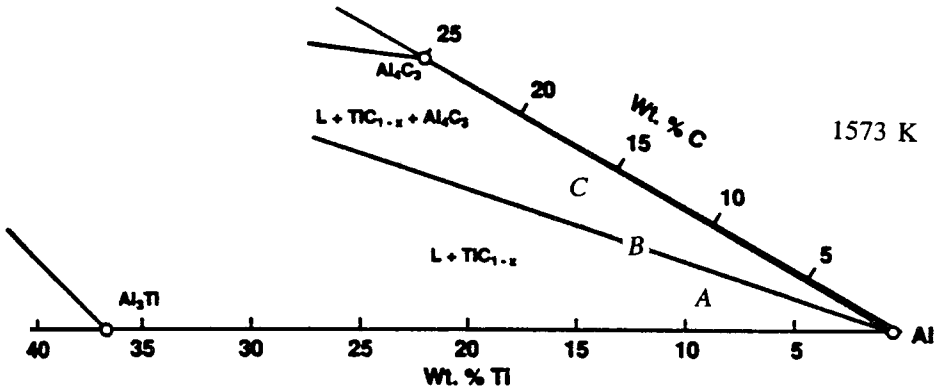

Figure 1 Illustration of an isothermal section of the Al-rich corner at 1573 K in the Al-Ti-C system.

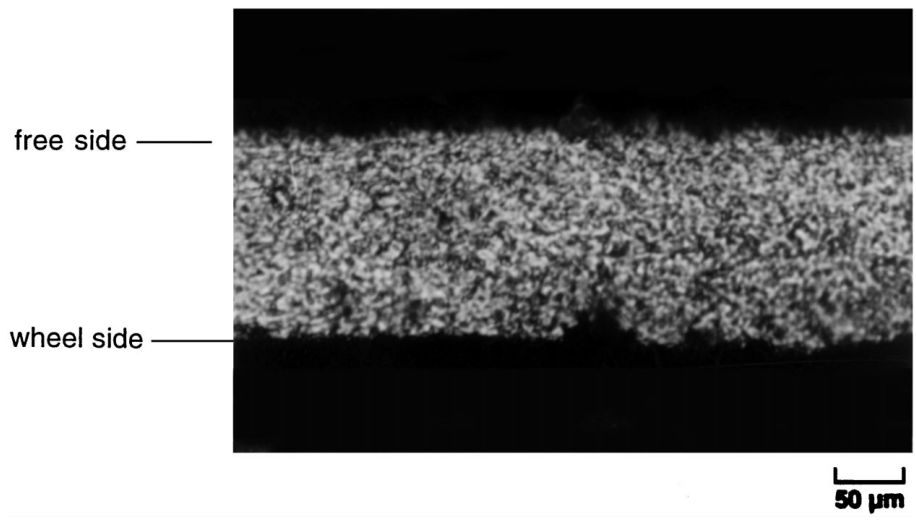

Figure 2 Optical micrograph of the cross-section of an rapidly solidified Al-4Ti-0.65C ribbons. No evident difference in the morphology of the grains between the wheel side and the free side of the ribbon.

TABLE I Typical compositions of Al-TiC composites, wt % (at %)

Master ingots	Ti	C	Fe	Si	C : Ti (at %)
Al-4Ti-0.65C	3.68(2.13)	0.65(1.49)	0.30	0.13	0.70
Al-7Ti-0.65C	7.23(4.25)	0.65(1.53)	0.30	0.13	0.36
Al-10Ti-1.2C	10.16(6.01)	1.15(2.58)	0.30	0.14	0.43
Al-12Ti-2.0C	12.01(7.10)	1.96(4.62)	0.34	0.14	0.65
Al-5Ti-1.0C	5.02(2.91)	1.04(2.33)	0.30	0.13	0.80
Al-6Ti-2.0C	6.07(3.48)	2.06(4.63)	0.30	0.13	1.33
Al-9Ti-3.0C	8.75(5.09)	2.85(6.76)	0.30	0.13	1.30

digitally after weight compensation and blank value correction.

Rapidly solidified samples were prepared in ribbon form by chill block melt spinning. A charge of 20 gram ingots was contained in a quartz crucible, and heated using high-frequency induction. A calibrated pyrometer was used to monitor melt temperatures. When the temperature rose to a given value (1623 K for 5 minutes), the melt was ejected through an orifice by argon gas at a pressure of 55 kPa onto the surface of a copper wheel rotating with a surface velocity of 30 m/s. The

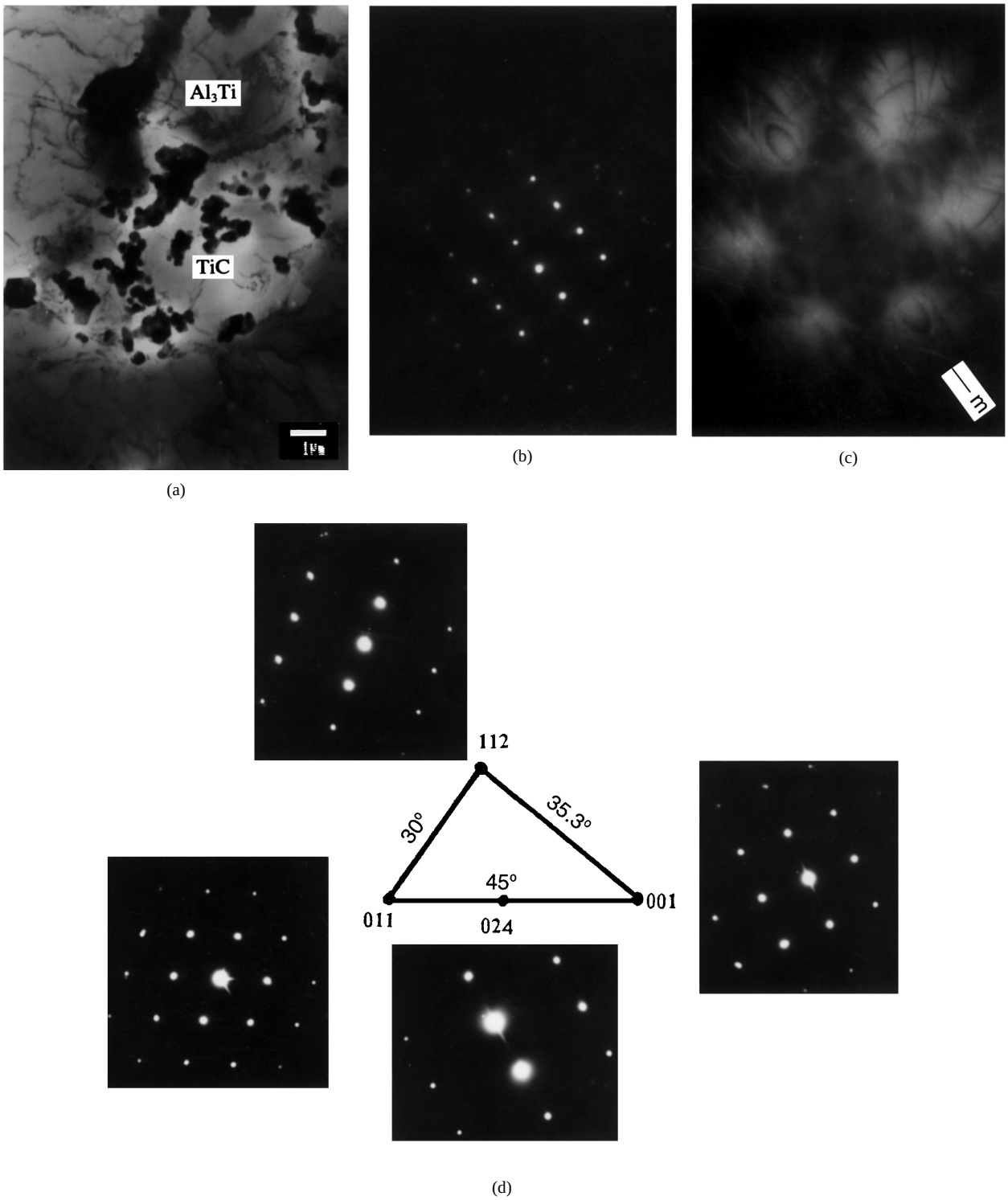

Figure 3 Direct chill casting microstructures of the Al-4Ti-0.65C ingot exhibits some needle-like Al_3Ti particles and another TiC particulate phase segregated generally at the grain boundaries (a); SAED (b) and CBED (c) patterns of $Al_3Ti\langle 101\rangle$; a series of diffraction patterns from TiC phase within the unit stereographic triangle (d).

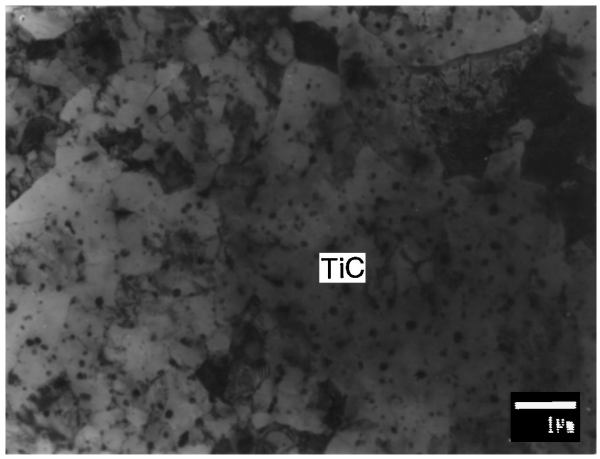

(a)

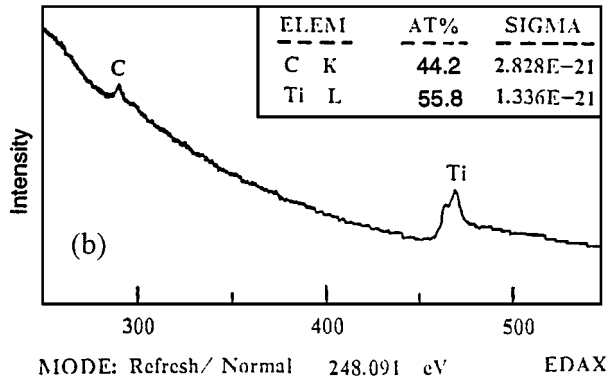

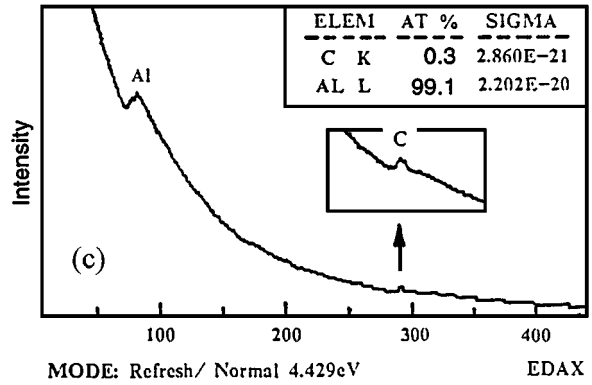

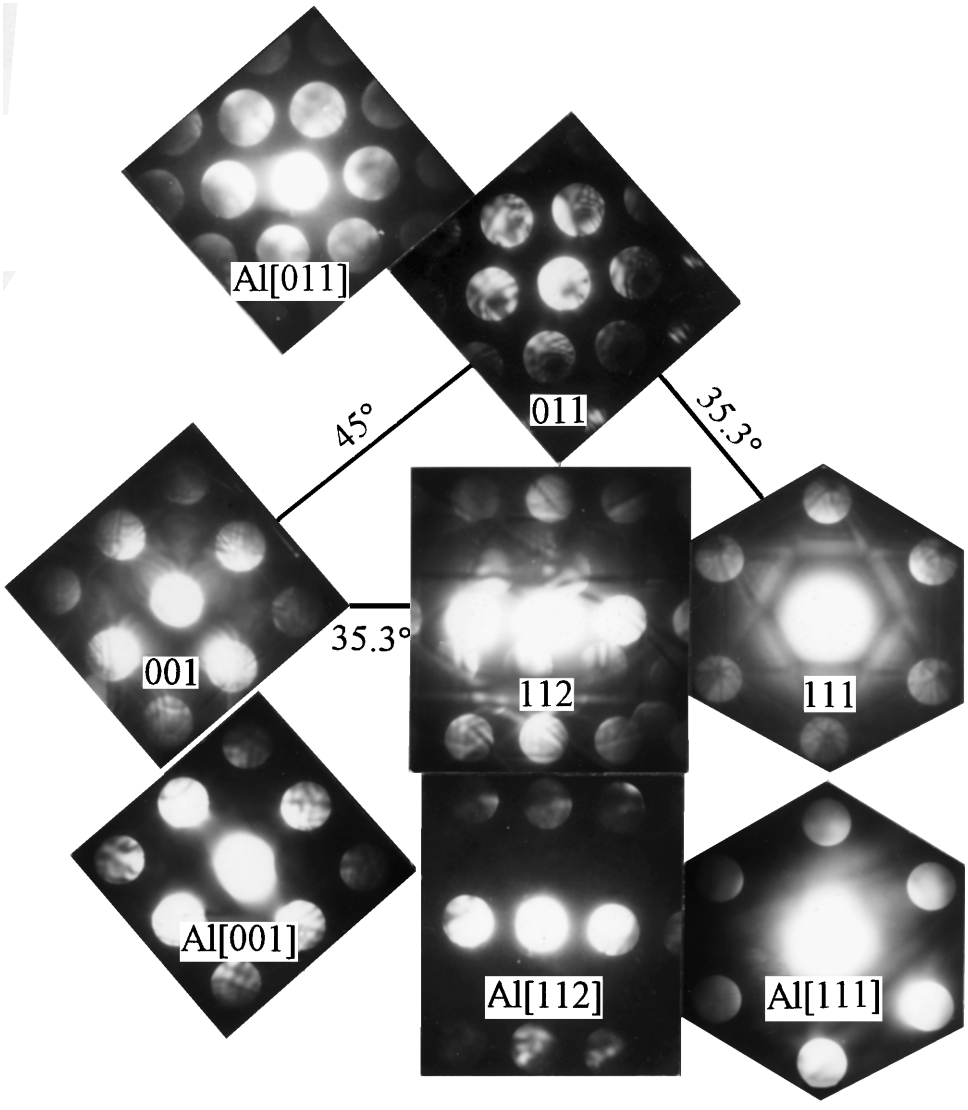

(d)

Figure 4 TEM microstructures of the rapidly solidified Al-4Ti-0.65C ribbons (a); EELS analysis data of the $TiC_{0.8}$ phase (b) and α-Al matrix (c); a series of microdiffraction patterns from the $TiC_{0.8}$ phase and the α-Al matrix within the unit stereographic triangle (d).

resultant ribbons were approximately 70–80 μm thick and 5 mm wide.

Samples for transmission electron microscopy (TEM) were punched mechanically from the ribbon and thinned to perforation by twin-jet electropolishing in a solution of 10 vol % perchloric acid, 10 vol % glycerin and 80 vol % ethanol. TEM examinations were performed in a JEOL-2000FX transmission electron microscope equipped with a Link AN-10000 energy dispersive X-ray spectrometer (EDS). Electron energy loss spectroscopy (EELS) analyses were carried out in a Philips CM12 transmission electron microscope equipped with a GATAN666 spectrometer. Standardless quantitative microanalysis was carried out using X-ray spectra acquired in scanning transmission electron microscopy mode and the energy dispersive X-ray analysis program THIN (EDAX laboratories, Prairie View, IL). The analysis were self-consistent and estimated accuracy of $\pm$10% on individual concentrations. X-ray diffraction of the ingot and ribbon were carried out using Philips PW1700 instrument with CuKα radiation.

Besides, standard metallographic techniques were employed to reveal the distribution of reinforcing phases and matrix phases. The volume fraction of the different micro-consistents (i.e., TiC, Al_3Ti, Al_4C_3, α-Al, etc.) was obtained from a series of point counts carried out in the optical and electron microscopes. The two-dimensional (2D) number density of approximately 1200 particles were counted in each case. These data were subsequently transformed into three-dimensional (3D) densities using the Saltykov analysis [25]. The specimens used in the middle of each section size in order to obtain comparable microstructural data in each case.

3. Results and discussion

The synthesis sequence of TiC under ordinary solidification conditions (near equilibrium) can be understood schematically by an isothermal section of the Al-Ti-C phase diagram shown in Fig. 1. This is an isothermal section schematic of the Al-rich corner at 1573 K [26], which can be divided into three zones. In the zone A, the solidification microstructure consists of TiC particles and Al_3Ti platelets due to unreacted Ti in the Al matrix. Near the line B, the reaction (Ti + C $\rightarrow$ TiC) is complete, i.e. all the Ti is consumed and the microstructure should consist of TiC particles in the Al matrix. If the overall composition is in zone C, in addition to TiC, Al_4C_3 platelets will appear in the microstructure. These platelets have been observed [17] and confirmed by the present work on the direct casting ingots. The rapid solidification of the ingots was found to produce a refinement of the microstructure insofar as the formation of the coarse, segregated phases was replaced by a dispersion of irregular, spheroidal particles distributed uniformly through nearly whole of the ribbon section. A representative optical micrograph of the rapidly solidified ribbons is shown in Fig. 2. There is no evident difference in the morphology of the grains between the wheel side and the free side of the ribbon. However, TEM study of the different ribbon samples revealed that the Al-TiC materials have different microstructures for various C : Ti atomic ratios, as will be shown later.

3.1. Al-4Ti-0.65C

The direct-chill-casting microstructures of the Al-4Ti-0.65C (zone A, C : Ti = 0.70) ingot exhibited some needle-like particles and another particulate phase which segregated generally at the grain boundaries, as shown in Fig. 3a. The former phase was identified as primary Al_3Ti (Fig. 3b and c); the latter phase consisted of agglomerates of fine particles usually of 0.2–1.0 μm size, and identified as TiC with the fcc crystal structure having a lattice parameter of 0.431 nm, as shown in Fig. 3d. In each diffraction pattern no evidence of superlattice reflections which should appear in the NaCl type crystal structure was found, indicating that the TiC formed in the present conditions might be a metastable disordered structure or the ordered domain sizes were too small to allow single domain diffraction [27]. Meanwhile, in order to determine the orientation relationship between intermetallic particles (Al_3Ti, TiC) and the α-Al matrix, diffraction patterns have been taken from these phases which also are in both sides of the phase boundaries. No consistent orientation relationships were found between any of these intermetallic phases and the matrix.

In the rapidly solidified Al-4Ti-0.65C ribbons, as shown in Fig. 4a, the precipitation of Al_3Ti phase was inhibited and TiC particles were refined and dispersed uniformly, with arrays of dislocation rings surrounding each individual TiC particles. The TiC particle diameter

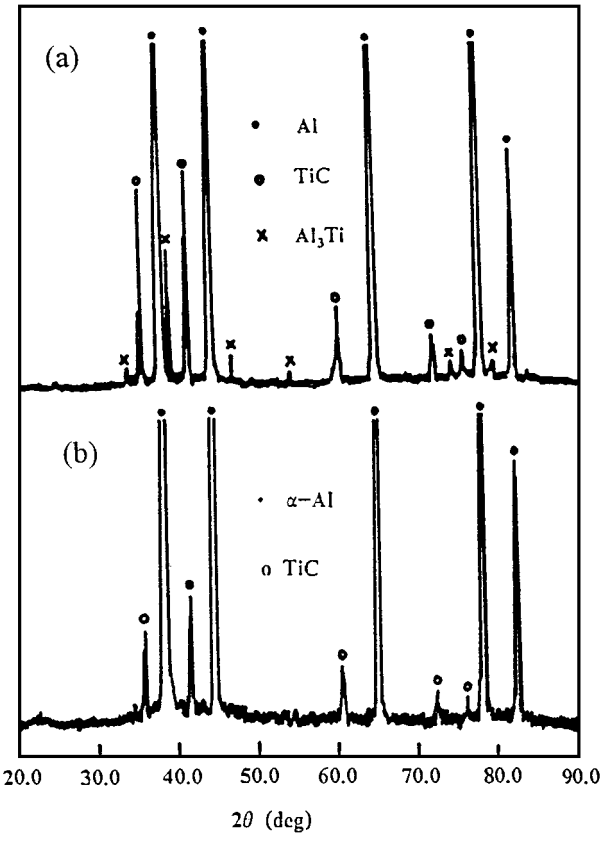

Figure 5 X-ray diffraction patterns of Al-4Ti-0.65C ingot (a) and ribbon (b).

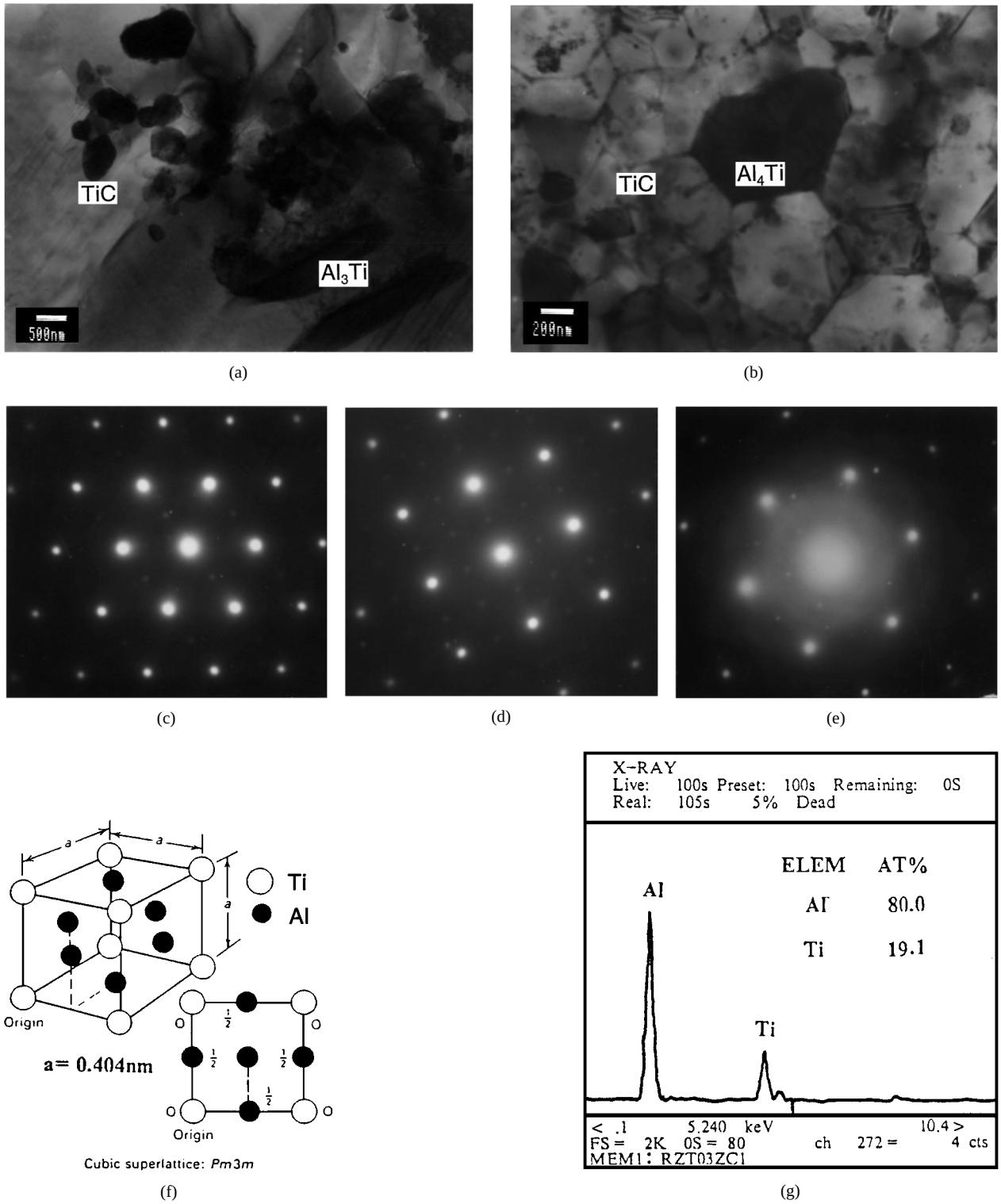

Figure 6 Direct chill casting microstructures of the Al-7Ti-0.65C ingot (a); rapidly solidified microstructures of Al-7Ti-0.65C ribbons (b), SEAD patterns of $\sim Al_4Ti$ [1 0 1] (c) [1 0 0] (d) [1 1 1] and (e) schematic of the $L1_2$ cubic superstructure (f), and EDS analysis pattern of the $\sim Al_4Ti$ phase in the ribbon (g).

varied from 10 to 80 nm. Fig. 4b shows EELS analysis results of these TiC particles, exhibiting an atomic composition of $TiC_{0.8}$ (the same as measured in the ingot casting samples [28]). Meanwhile, the EELS analysis result (Fig. 4c) shows that the Ti and C contents supersaturated in the α-Al matrix were approximately 0.6 at % and 0.3 at %, respectively. Fig. 4(d) shows a series of microdiffraction patterns taken from the dispersed TiC particles, also identified as fcc type crystal structure with a lattice parameter of 0.431 nm. Unlike in the ingot casting samples, the microdiffraction analyses of α-Al matrix near all of the TiC particles in the ribbons show that a cube-cube orientation relationship was present between TiC dispersoids and the matrix. And moreover, a disregistry δ between TiC and α-Al could be calculated as $\delta = (0.431 - 0.405)/0.431 = 0.060$. This showed that the TiC phase has a coherent or near coherent interface with α-Al matrix. Therefore, the TiC particles may act as the active nucleation sites of α-Al during solidification. Meanwhile, these phases were

confirmed by the X-ray diffraction analyses shown in Fig. 5.

3.2. Al-7Ti-0.65C

The increase of the Ti solute content in the Al-7Ti-0.65C (zone A, C : Ti = 0.36) resulted in changes in the microstructure. In the ingot castings, the number of the needle-like Al_3Ti particles increased, though the distribution of the TiC particles is the same as that in the Al-4Ti-0.65C (Fig. 6a). Meanwhile, the rapidly solidified microstructure was composed of microgranulars (0.30–0.75 μm in diameter) with grain boundaries decorated with fine, spheroidal intermetallic phase particles (20–80 nm in diameter) while a few of these particles remained in the α-Al grains, as shown in Fig. 6b. EELS and microdiffraction analyses indicated that these grain boundary particles were TiC with similar composition to the one in Al-4Ti-0.65C ingot and ribbons. However, no consistent crystal orientation relationship was found between most of these TiC particles and the α-Al matrix.

In addition to the TiC phase dispersions, the rapidly solidified microstructure contained a coarser scale dispersion of cuboidal particles. These particles were typically 0.1–0.3 μm in size and generally distributed on each α-Al grain in an individual single particle, as if they formed as primary phase particles directly from the melt and played a role of heterogeneous sites of α-Al phase during rapid solidification. EELS and EDS analysis of these particles indicate that they are only comprised of Al and Ti elements, with an approximate composition of $\sim Al_4Ti$ (Fig. 6g). Fig. 6c, d and e show electron diffraction patterns from the cuboidal phase, indexed as the ordered $L1_2$ crystal structure with a lattice parameter $a_0 \approx 0.404$ nm [29]. Compared with the ingot casting, the formation of the equilibrium intermetallic phase Al_3Ti was suppressed and replaced by the metastable $\sim Al_4Ti$ phase formed during rapid solidification. Moreover, the metastable cuboidal phase particles share an identity orientation relationship and a low lattice misfit with the α-Al matrix phase. A disregistry δ between $\sim Al_4Ti$ and α-Al can be calculated as $\delta = (0.404 - 0.405)/0.404 = 0.003$, showing a coherent interface relationship between $\sim Al_4Ti$ and the α-Al matrix. This seems to indicate that the heterogeneous sites of α-Al phase are probably $\sim Al_4Ti$ instead of TiC in the rapidly solidified Al-7Ti-0.65C ribbons. And moreover, the slight difference of the lattice parameter values between $\sim Al_4Ti$ and α-Al might resulted in that the $\sim Al_4Ti$ phase could not been clearly distinguished with α-Al phase in the X-ray diffraction patterns, as shown in Fig. 7.

The microstructural characteristics of Al-10Ti-1.2C and Al-12Ti-2.0C ingots and ribbons are the same as the ones of the Al-7Ti-0.65C.

3.3. Al-5Ti-1C

The increase of both the Ti and C contents up to an atomic ratio C : Ti = 0.80, which corresponded to the atomic composition of the $TiC_{0.8}$ formed in the composites, produced predictable results. Fig. 8a exhibits

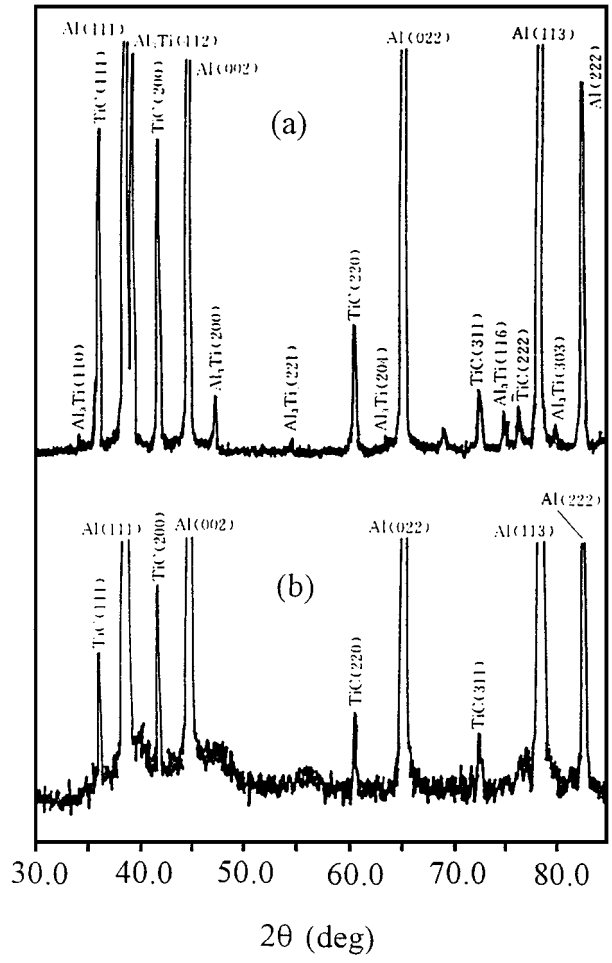

Figure 7 X-ray diffraction patterns of Al-7Ti-0.65C ingot (a) and ribbon (b).

the direct chill casting microstructure of the Al-5Ti-1C ingot. A high volume fraction of TiC particles are distributed within the matrix, while the Al_3Ti phase particles are no longer observed. This indicates that the solute elements Ti and C completely reacted to form TiC particles or some of them remained in solution. As that in the Al-4Ti-0.65C and Al-7Ti-0.65C ingots, the accumulated TiC particulate phase comprised fine particles usually of 0.2–1.0 μm size, in which the larger were polyhedral-shaped while the smaller were globular. The rapidly solidified microstructure was distinctly microcellular in nature, as shown in Fig. 8b. However, the distribution of the dispersed TiC particles was similar to that of the Al-4Ti-0.65C ribbons except the evident increase in particle volume fraction. Moreover, the TiC phase particles, located on both intercellular and intracellular, all shared an identity orientation relationship with the α-Al matrix phase. The phase mixtures of the Al-5Ti-1C ingot and ribbons were confirmed by X-ray diffraction analysis, as shown in Fig. 8c and d.

3.4. Al-6Ti-2C

As the atomic ratio C : Ti is increased up to 1.33, similar microstructural characteristics to the Al-5Ti-1C alloy are observed except for the appearance of Al_4C_3 phase particles. In the direct chill casting ingots, as shown in Fig. 9a, a high volume fraction of accumulated TiC particles is distributed in the α-Al matrix and

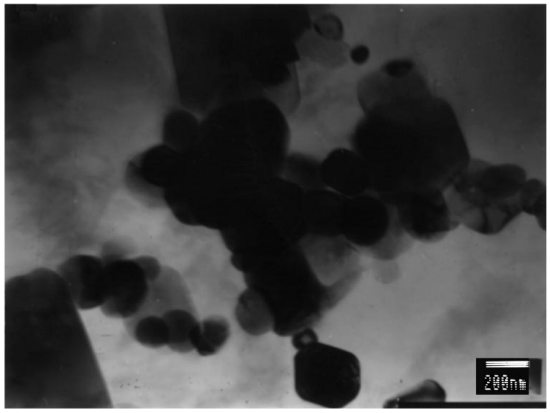

(a)

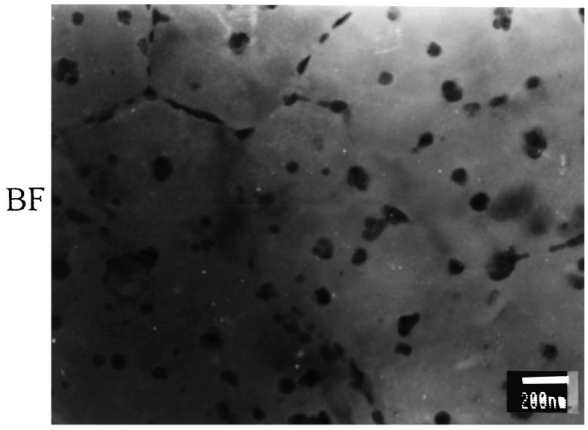

(b)

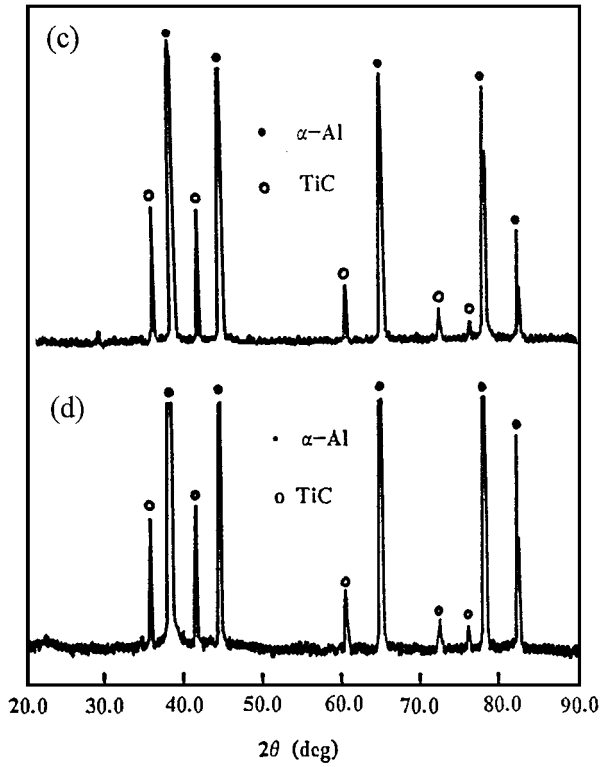

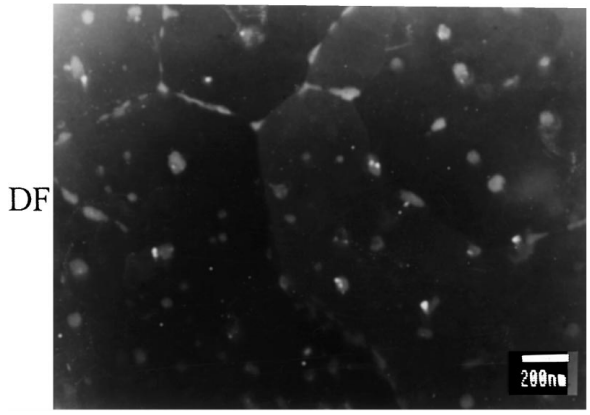

(e)

Figure 8 Direct chill casting microstructures of the Al-5Ti-1C ingot (a); rapidly solidified microstructures of Al-5Ti-1C ribbons: bright field (b) and centered dark field (c); and X-ray diffraction patterns of Al-5Ti-1C ingot (d) and ribbon (e).

the Al_4C_3 phase plates appeared in some regions of α-Al matrix. Fig. 9b shows that the microstructure of the Al-6Ti-2C ribbons are similar to those of the Al-5Ti-1C ribbons except a higher volume fraction of dispersoid particles are present, which include mostly TiC and some remained Al_4C_3 phase particles. Most of TiC phase particles have an exact crystal orientation relationship with α-Al matrix. The above results were confirmed by X-ray diffraction analysis, as shown in Fig. 9c and d. In the same C : Ti atomic ratio, much higher volume fraction of TiC could be obtained in the Al-9Ti-3C

TABLE II The volume fractions (vol %) of TiC, Al_3Ti and Al_4C_3 in the DC casting ingots of the experimental materials

Master ingots	C : Ti (at %)	TiC	Al_3Ti	Al_4C_3
Al-4Ti-0.65C	0.70	8.5	3.4	—
Al-7Ti-0.65C	0.36	7.5	9.3	—
Al-10Ti-1.2C	0.43	10.0	20.0	—
Al-12Ti-2.0C	0.65	18.0	16.0	—
Al-5Ti-1.0C	0.80	14.5	—	—
Al-6Ti-2.0C	1.33	16.0	—	8.5
Al-9Ti3.0C	1.30	25.0	—	9.0

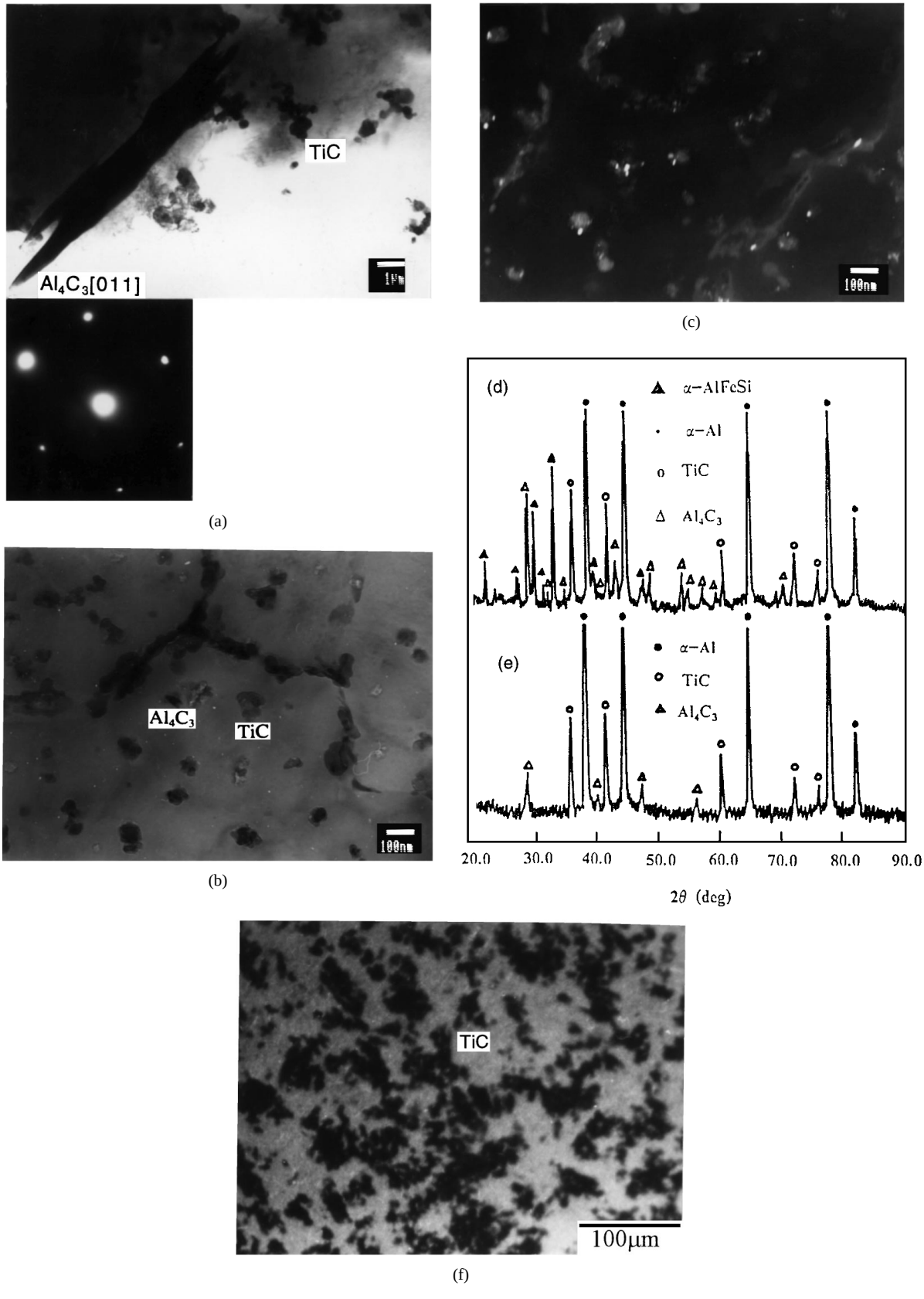

Figure 9 Direct chill casting microstructures of Al-6Ti-2C ingot (a); rapidly solidified microstructures of Al-6Ti-2C ribbons: bright field (b) and centered dark field (c); X-ray diffraction patterns of Al-6Ti-2C ingot (c) and ribbon (d); and the optical image of direct chill casting microstructures of Al-9Ti-3C ingot (e).

by raising the amount of both Ti and C, as shown in Fig. 10.

The key quantitative analysis results of the above experimental materials from the microstructures are summarized in Tables II and III for the direct chill casting ingots and RS ribbons, respectively. Based on the Fullman's theory [30] for a polydispersed system of spheres, the measured 2D diameters (d_a) can be converted into 3D values (d_v) through the relation $d_v = \pi d/2$, therefore, it is possible to estimate the total number of particles per unit volume (N_v) when the particle volume fraction is measured: $N_v = 6V_f/[\pi(d_v)^3]$.

TABLE III Key results of microstructures of the RS materials

Materials	Matrix grains			TiC particles				Al_4Ti		Al_4C_3
	d_m	C_{Tid}	C_{cd}	d_a	d_v	N_v	V_f	V_f	N_v	V_f
Al-4Ti-0.65C	0.65	0.6	0.3	60	94	1.72×10^{11}	7.5			
Al-7Ti-0.65C	0.53	1.0	0.3	50	79	2.52×10^{11}	6.5	10.7	1.18×10^{10}	
Al-10Ti-1.2C	0.55	0.6	0.3			1.32×10^{12}	15.5	10.7	1.18×10^{10}	
Al-12Ti-2.0C	0.55	0.6	0.3			2.43×10^{12}	28.0	10.7	1.18×10^{10}	
Al-5Ti-1.0C	0.55	0.3	0.3	40	63	1.03×10^{12}	13.5			0.03
Al-6Ti-2.0C	0.45	—	< 0.3	36	57	1.65×10^{12}	16.0			8.80

*$d_v = \pi d/2$, $N_v = 6V_f/[\pi(d_v)^3]$[30]. d_a: arithmetic mean 2D particle diameter; d_v: arithmetic mean 3D particle diameter; d_m: mean matrix grain diameter; V_f: particle volume fraction; N_v: number of particles per unit volume; C_{id}: solute of species i in the matrix.

4. Conclusion

Combining the advantages of ingot metallurgy, rapid solidification and *in situ* synthesis of composites, a kind of innovative *in situ* processing of Al-TiC composites has been developed by optimizing selection of material compositions and processing parameters. The important observations are listed below.

1. In the ingot metallurgy and rapidly solidified Al-TiC composites, a single $TiC_{0.8}$ phase distribution in the matrix has been formed when the initial C : Ti ratio is in the vicinity of 0.8. The *in situ* synthesized $TiC_{0.8}$ particles possess a metastable fcc crystal structure with a lattice parameter of 0.431 nm. If the $C : Ti \ll 0.8$, the second phase is composed of the TiC particulate phase and the needle-like Al_3Ti particle phase or cubic $\sim Al_4Ti$ particle phase in the rapidly solidified samples; if the $C : Ti \gg 0.8$, the second phase consists of TiC phase and needle-like Al_4C_3 phase and the volume fraction of TiC particles increases from 8.5 to 16.0 vol % (even up to 20.0 vol % in ingot Al-TiC composites) with increasing the initial C, Ti contents.

2. The typical microstructures of ingot metallurgy Al-TiC composites exhibit the agglomerated TiC phase which accumulates at the α-Al subgrain or grain boundaries and consists of fine particles of 0.2–1.0 μm, in which the larger has a polyhedral morphology while the smaller is round or globular.

3. In comparison, the typical rapidly solidified microstructures formed under certain thermal history conditions consist of a uniform fine-scale dispersion of TiC phase particles with size of 40–80 nm in an α-Al supersaturated matrix of 0.30–0.85 μm grain size and the TiC dispersed particles generally have a semicoherent relationship with the α-Al matrix.

References

1. S. V. NAIR, J. K. TIEN and R. C. BATES, *Int. Meter. Rev.* **30** (1985) 275.
2. V. C. NARDONE and K. W. PREWO, *Scripta Metall.* **20** (1986) 43.
3. I. A. IBRAHIM, F. A. MOHAMED and E. J. LAVERNIA, *J. Mater. Sci.* **26** (1991) 1137.
4. P. K. ROHATGI, *Key Eng. Mater.* **104–107** (1995) 293.
5. A. CHRYSANTHOU, *ibid.* **104–107** (1995) 381.
6. T. Z. KATTAMIS and T. SUGANUMA, *Mater. Sci. Eng.* **A128** (1990) 241.
7. R. MEHRABIAN, *MRS Symp.* **120** (1988) 3.
8. T. W. CLYNE and J. F. MASON, *Metall. Trans.* **18A** (1987) 1519.
9. Y. WU and E. J. LAVERNIA, *ibid.* **23A** (1992) 2923.
10. A. R. C. WESTWOOD, *ibid.* **19B** (1988) 155.
11. Martin Marietta Corp., US Pat. 4915908, 1990.
12. P. SAHOO and M. J. KOCZAK, *Mater. Sci. Eng.* **A114** (1991) 37.
13. I. GOTMAN, M. J. KOCZAK and E. SHTESSEL, *ibid.* **A187** (1994) 189.
14. A. BERGMAN, A. JARFORS, Z. LIU and H. FREDRIKSSON, *Key Eng. Mater.* **79–80** (1993) 213.
15. C. RAGHUNATH, M. S. BHAT and P. K. ROHATGI, *Scripta Metall. Mater.* **32** (1995) 577.
16. M. J. KOCZAK and K. S. KUMAR, US Pat. 4808372, 1989.
17. M. K. PREMKUMAR and M. G. CHU, *Metall. Trans.* **24A** (1993) 2358.
18. P. K. ROHATGI, R. ASTHANA and F. YARANDI, in "Solidification of Metal Matrix Composites," edited by P. K. Rohatgi (TMS, Warrendale, PA, 1990) p. 51.
19. A. MORTENSEN, J. A. CORNIE and M. C. FLEMINGS, *Metall. Trans.* **19A** (1988) 709.
20. J. D. BRIANT, J. R. MAISANO, D. T. WINTER and A. R. H. BARRETT, *Scripta Metall.* **24** (1990) 2209.
21. A. MORTENSEN, in "Solidification of Metal Matrix Composites," edited by P. K. Rohatgi (TMS, Warrendale, PA, 1990) p. 1.
22. D. M. STEFANESCU, A. MOITRA, A. S. KACAR and B. K. DHINDAW, *Metall. Trans.* **21A** (1990) 231.
23. R. ASTHANA, S. DAS, T. K. DAN and P. K. ROHATGI, *J. Mater. Sci. Lett.* **5** (1986) 1083.
24. T. S. SRIVATSAN and T. S. SUDARSHAN, in "Rapid Solidification Technology," edited by T. S. Srivatsan and T. S. Sudarshan (Technomic Publishing Company, Western Hemisphere, 1993) p. 603.
25. E. E. UNDERWOOD, "Quantitative Stereology" (Addison-Wesley Publishing Co., London, 1970).
26. F. H. HAYES, in "Ternary Alloys," edited by A. Petzow and G. Effenberg (VCH Publishers, New York, NY, 1990) p. 557.
27. V. MOISY-MAURICE, N. LORENZELLI, C. H. DE NOVION and P. CONVERT, *Acta Metall.* **30** (1982) 1769.
28. X. C. TONG and H. S. FANG, *J. Alloys and Compounds* **239** (1996) 203.
29. J. F. NIE, S. SRIDHARA and B. C. MUDDLE, *Metall. Trans.* **23A** (1992) 3193.
30. R. L. FULLMAN, *Trans. AIME.* **197** (1953) 447.

Received 20 November 1997
and accepted 14 September 1998